View Article Online
DOI: 10.1039/C4TA05974C

Synthesis and properties of push-pull porphyrins as sensitizers for NiO based dye-sensitized solar cells

Antoine Maufroy,[ab] Ludovic Favereau,[a] Frédéric B. Anne,[a] Yann Pellegrin,[a] Errol Blart,[a] Muriel Hissler,[b] Denis Jacquemin,*[ac] Fabrice Odobel*[a]

[a]*Université LUNAM, Université de Nantes, CNRS, Chimie et Interdisciplinarité: Synthèse, Analyse, Modélisation (CEISAM), UMR 6230,2 rue de la Houssinière, 44322Nantes cedex 3, France. E-mail: Fabrice.Odobel@univ-nantes.fr; Fax: +33 251125402; Tel: +33 251125429*

[b]*Institut des sciences chimiques de Rennes - UMR 6226 263 Avenue du General Leclerc CS 74205 35042 Rennes cedex, France.*

[c]*Institut Universitaire de France, 103 blvd St Michel, 75005 Paris Cedex 5, France. E-mail: Denis.Jacquemin@univ-nantes.fr*; Fax: +33 251125567; Tel: +33 251125564.

Abstract

Zinc porphyrins derivatives were prepared and investigated in NiO-based p-type dye sensitized solar cells. The first series consist of *trans* disubstituted push-pull porphyrins containing a nitrophenyl unit as electron withdrawing group and a benzoic acid unit as anchoring group. An ethynyl spacer was introduced between the porphyrin *meso* positions and the nitrophenyl or/and the benzoic acid. In a second series a secondary electron acceptor such as benzyl-viologen or a naphthalene diimide was appended to the porphyrin. All the compounds were characterized by absorption and emission spectroscopies, theoretical calculations and by electrochemistry. The fast charge recombination certainly limits the photovoltaic performances of the first series, which remain modest (Jsc ≈ 0.5 mA/cm^2, Voc≈ 110 mV, ff ≈ 36% and PCE ≈ 0.02%) compared to highly performing sensitizers for NiO.

View Article Online
DOI: 10.1039/C4TA05974C

However, promising performances (Jsc = 1.38 mA/cm^2, Voc= 127 mV, ff = 32%, PCE=0.038%) were recorded for the dyad with naphthalene diimide.

Introduction

The conversion of sunlight into electricity is an attractive environmentally friendly strategy to satisfy the increasing energy need of mankind. Among several photovoltaic technologies, particular attention has been devoted to dye sensitized solar cells (DSCs).[1] In a classical DSC, using TiO_2 as inorganic n-type semiconductor (n-SC), the working principle lies in the electronic transfer from the electronically excited state of the molecular dye into the conduction band of the semi-conductor. In p-DSCs, employing a p-type inorganic SC such as NiO, the operation principle is just the opposite as that of n-DSCs since photoexcitation of the sensitizer is accompanied by hole injection into the valence band (VB) of the p-SC.[2] The solar energy conversion in electricity (or PCE for Power Conversion Efficiency) of the records n-DSC are as high as 12-13%.[3, 4] Whilst this PCE is significantly large, its progression has been rather slow for several years, especially when compared to emerging technologies such as perovskite-based solar cells[5] or organic photovoltaic.[6, 7] An elegant way to enhance the PCE of DSC is to build tandem DSC (pn-DSC) where the photo-inert platinum counter electrode is substituted by a photocathode consisting of a dye sensitized p-type SC, such as NiO.[2, 8-11] Those pn-DSCs have the potential to harvest a larger portion of the sunlight spectrum and consequently to reach much higher PCE than n-DSC. The development of pn-DSC is quite recent and only a small (but increasing) number of scientific contributions have appeared in the field.[10-13] Today, the PCEs of pn-DSC, are however still lower than conventional n-DSCs (the record PCE is 2.42%),[10] essentially due to the modest efficiency of the current photocathodes. To advance in the development of better performing photocathodes, new sensitizers are needed. Porphyrins are valuable dyes for solar energy conversion applications since their derivatives are the ubiquitous light collectors in biological photosynthetic organisms (chlorophyll is the main chromophore in the

View Article Online
DOI: 10.1039/C4TA05974C

photosynthetic reaction centre and light harvesting antenna) and they are very active dyes in conventional n-DSCs[3, 4, 14, 15] and organic solar cells.[16, 17] Furthermore, porphyrins absorb intensively light on a broad wavelength domain and simple chemical transformations enable to tune their electronic properties to a large extent. These valuable properties prompted us to optimize porphyrin dyes to develop efficient sensitizers for NiO based p-DSC. We indeed felt that this class of dyes was under-investigated for these applications and they can certainly lead to high PCE in p-DSCs. Indeed, to the best of our knowledge, there are only three reports of porphyrin sensitizers used p-DCSs.[18-20] Towards this objective, we have selected push-pull systems because this type of structures exhibits charge transfer (CT) transitions, which are particularly well suited to induce charge transfer reactions and in general push-pull dyes proved to be highly performing both in n-DSCs[21] and p-DSC.[22, 23] In the present study, zinc porphyrins bear a benzoic acid as anchoring moiety and a nitrophenyl as electron withdrawing unit (Chart 1). These subunits are placed in *trans* within a tetraaryl porphyrin and an ethynyl unit was introduced between a zinc porphyrin and the *meso* aryl substituents to create push pull dyes (Chart 1).

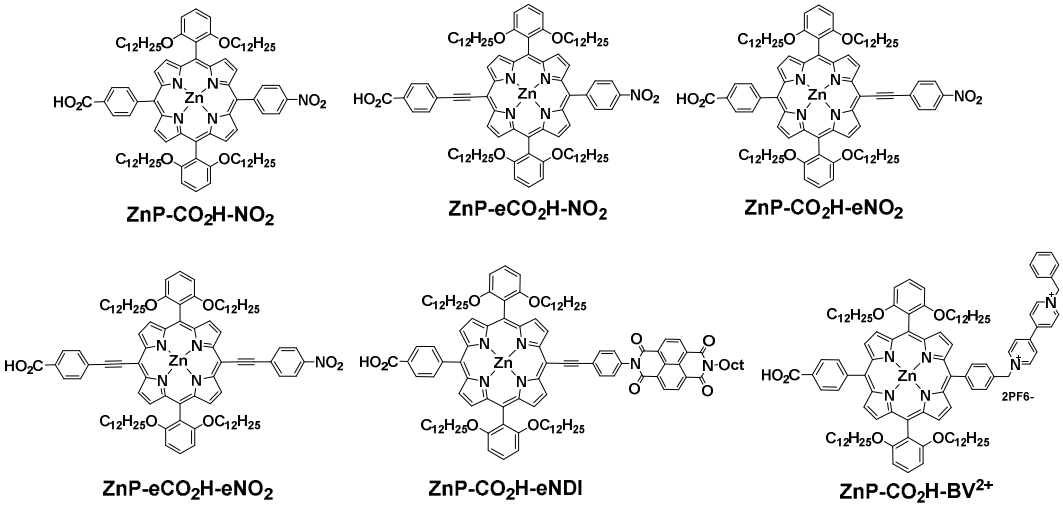

Chart 1. Structures of the porphyrins described in this work.

View Article Online
DOI: 10.1039/C4TA05974C

Porphyrins were also functionalised by two alkoxy phenyl substituents. Those lipophilic alkoxy chains enable to decrease the aggregation tendency of these planar aromatic systems and to passivate the SC surface by impeding the approach of the redox mediator from the NiO surface.[24] In a second series of sensitizers, a secondary electron acceptor (viologen: BV^{2+} or naphthalene diimide: NDI) was appended to the porphyrin in order to enhance the charge separated state lifetime because this type of construction proved to be efficient for such purpose.[10, 25, 26] Detailed synthesis, physico-chemistry characterisations and photovoltaic performances are presented in this contribution and the results will be rationalised with the help of Time-Dependent Density Functional Theory (TD-DFT) calculations. It is shown that the fast charge recombination reaction is the main factor which limits the performances of this class of dyes. However, the introduction of a secondary electron acceptor in the vicinity of the porphyrin can heal this drawback and this strategy can certainly be used to take full advantage of the light harvesting properties of porphyrin derivatives.

Experimental part

Theoretical calculations

All simulations have been achieved with the Gaussian09 program[27], using Density Functional Theory (DFT) and Time-Dependent DFT, for the ground and excited state properties, respectively. The computational protocol proceeds through a four step strategy that is efficient to determine the charge transfer features of rod-like organic dyes: 1) the ground-state geometrical parameters have been determined at the PBE0/6-31G(d) level[28] [LanL2DZ pseudo-potential and basis set for Zn], via a force-minimization process using a SCF convergence threshold of at least 10^{-9} a.u.; 2) the vibrational spectrum of each derivative has been determined analytically at the same level of theory, that is PBE0/6-31G(d) [LanL2DZ for Zn], and it has been checked that all structures correspond to true minima of the potential energy surface; 3) the first fifteen low-lying excited-states have been determined within the vertical TD-DFT approximation using the CAM- B3LYP/6-31+G(d)[29] [LanL2DZ

View Article Online
DOI: 10.1039/C4TA05974C

for Zn] level of approximation with a tight SCF convergence threshold (at least 10^{-7} a.u.); 4) the charge-transfer parameters have been estimated with the procedure defined by Le Bahers[30] and coworkers using the CAM-B3LYP electronic densities. It proposes to evaluate the distance separating the barycenters of the electron density gain/depletion upon electron transition. All calculations systematically include a modelling of bulk solvent effects (here dichloromethane) through the Polarizable Continuum Model (PCM)[31]. During the simulations, the long alkyl chains have been replaced by methyl groups (e.g., the $OC_{12}H_{25}$ have been replaced by methoxy groups) in order to lighten the computational burden.

Synthesis

Porphyrin **ZnP-eCO_2H-eNO_2** was prepared from the already published dibromo zinc porphyrin **1**[32] following two consecutive Sonogashira's cross coupling reactions, first with (4-nitro-phenyl)ethynyl **2** and then with (4-carboxy-phenyl)ethynyl **4** according to Lindsey copper-free conditions (Scheme 1).[33] The intermediate bromo (4-nitro-phenyl)ethynyl porphyrin **3** was used again to prepare **ZnP-CO_2H-eNO_2**. **3** was subjected to a Suzuki cross-coupling reaction with the commercially available 4-methoxycarbonylphenylboronic acid **5** followed by basic hydrolysis to furnish **ZnP-CO_2H-eNO_2** in 51% yield (Scheme 1).

View Article Online
DOI: 10.1039/C4TA05974C

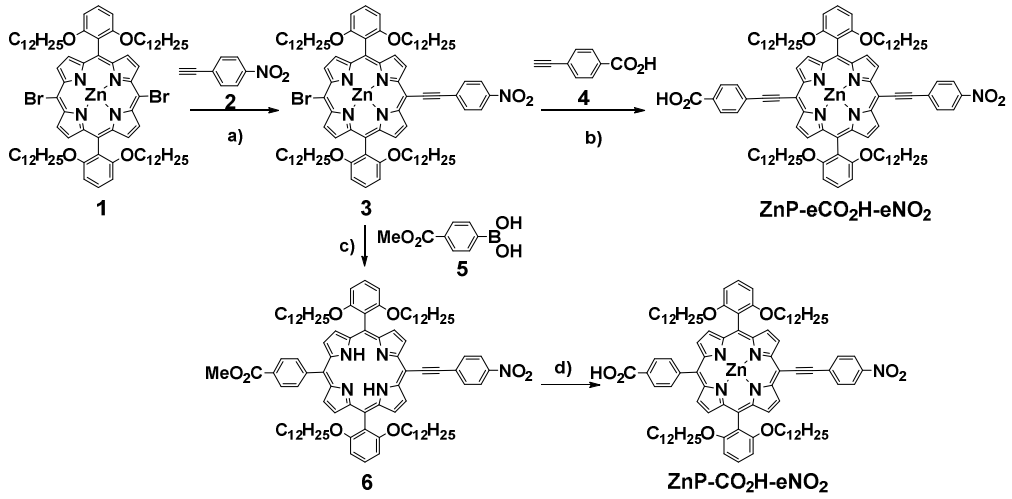

Scheme 1. Synthesis of the porphyrins ZnP-eCO$_2$H-eNO$_2$ and ZnP-CO$_2$H-eNO$_2$. Reagents and conditions: a) $Pd(PPh_3)_4$, CuI, Et_3N, THF, reflux; yield: 17%, b) $Pd_2(dba)_3$, $AsPh_3$, Et_3N, THF/MeOH (v/v: 1/1), reflux; yield: 30%, c) $Pd(PPh_3)_4$, $Ba(OH)_2.H_2O$, THF/H_2O (v/v: 3/1), reflux followed by acidic treatment; yield: 51%, d) $Zn(OAc)_2.4\ H_2O$, CH_2Cl_2/MeOH (v/v: 1/1), reflux followed by NaOH (1M), THF/MeOH (v/v: 8/1), reflux; yield: 100%.

ZnP-eCO$_2$H-NO$_2$ was prepared from the monoiodo trisisopropyl-ethynyl porphyrin **7** which was already reported in literature.[34] A first Suzuki's cross coupling reaction with the commercially available nitrophenyl boronic acid **8** with porphyrin **7** followed by deprotection of the TIPS group by fluoride anion and a final Sonogashira's cross coupling reaction using copper-free conditions gave **ZnP-eCO$_2$H-NO$_2$** with an overall yield of 45% (Scheme 2). **Zn-CO$_2$H-NO$_2$** was prepared from the known mono-brominated porphyrin **11**[34] according to two consecutive Suzuki's cross couplings. First, the porphyrin **11** was reacted with 4-methoxycarbonylphenyl boronic acid **5** and then the resulting coupled product **12** was brominated with NBS to afford the key intermediate **13** in high overall yield (94%). The latter serves as starting material for the synthesis of **ZnP-CO$_2$H-NO$_2$**, **ZnP-CO$_2$H-eNDI** and **ZnP-CO$_2$H-BV^{2+}**. The porphyrin **13** was subjected to a Suzuki cross-coupling reaction with the nitrophenyl boronic acid **8** followed by basic hydrolysis and metallation with zinc acetate to furnish **ZnP-CO$_2$H-NO$_2$** with a 67% overall yield (Scheme 2).

View Article Online
DOI: 10.1039/C4TA05974C

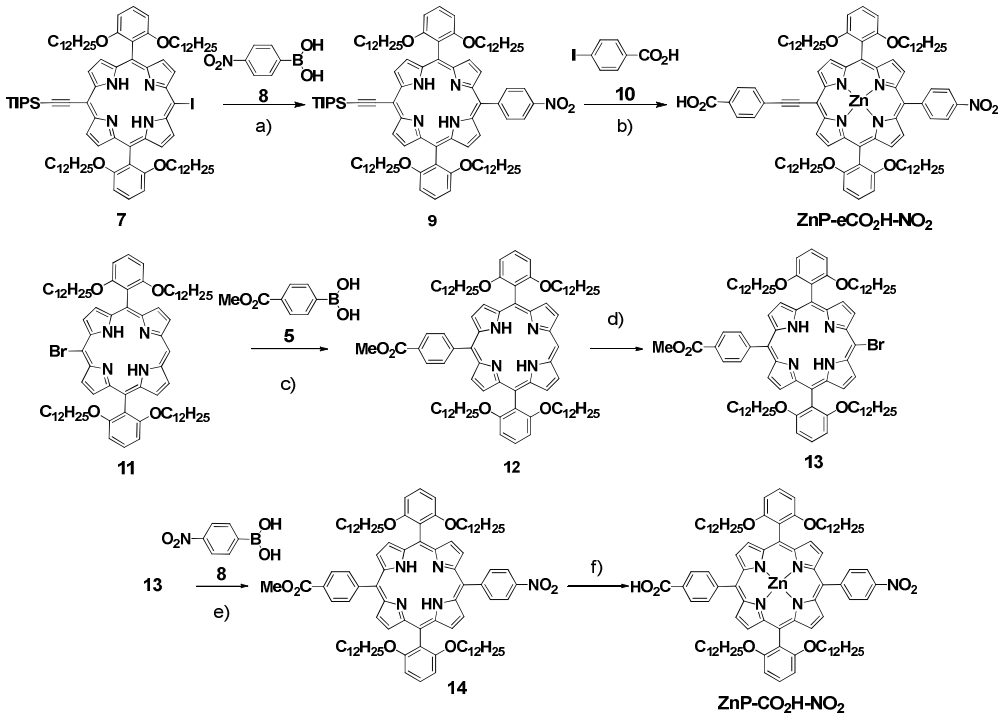

Scheme 2. Synthesis of the porphyrins **ZnP-eCO$_2$H-NO$_2$ and ZnP-CO$_2$H-NO$_2$**. Reagents and conditions: a) Pd(PPh$_3$)$_4$, Ba(OH)$_2$.H$_2$O, THF/H$_2$O (v/v: 3/1), reflux; yield: 48%, b) Zn(OAc)$_2$.4 H$_2$O, CH$_2$Cl$_2$/MeOH (v/v: 1/1), reflux followed by TBAF, THF, rt then Pd$_2$(dba)$_3$, AsPh$_3$, Et$_3$N, THF, reflux; yield: 95%, c) Pd(PPh$_3$)$_4$, Ba(OH)$_2$.H$_2$O THF/H$_2$O (v/v: 3/1), reflux; yield: 99%, d) NBS, CHCl$_3$, rt; yield: 94%, e) Pd(PPh$_3$)$_4$, Ba(OH)$_2$.H$_2$O, THF/H$_2$O (v/v: 3/1), reflux; yield: 68%, f) aqueous NaOH (1M), THF/MeOH (v/v: 8/1), reflux followed by Zn(OAc)$_2$.4 H$_2$O, CH$_2$Cl$_2$/MeOH (v/v: 1/1), reflux; yield: 99%.

For the synthesis of the dyads, the methyl carboxylic ester of porphyrin **13** was first hydrolysed with aqueous sodium hydroxide. The carboxylic acid free-base porphyrin **15** was then metalated with zinc acetate and subsequently coupled with the known ethynyl-NDI **16**[6, 35] according to the Sonogashira cross-coupling conditions to afford **ZnP-CO$_2$H-eNDI** in 68% yield (Scheme 3). The second dyad was prepared according to a Suzuki's cross coupling reaction between porphyrin **15** and 1-(borolan)benzyl bipyridinium salt **19**. The latter was synthesized by nucleophilic substitution of 4-4'-bypyridine and the commercially available (Bromomethyl)benzeneboronic acid pinacol ester **18** in good yield (77%). Finally, the benzylation of the second pyridine fragment of porphyrin **20** by an excess of benzyl bromide afforded the desired dyad **ZnP-CO$_2$H-BV^{2+}** in 75% yield (Scheme 3).

View Article Online
DOI: 10.1039/C4TA05974C

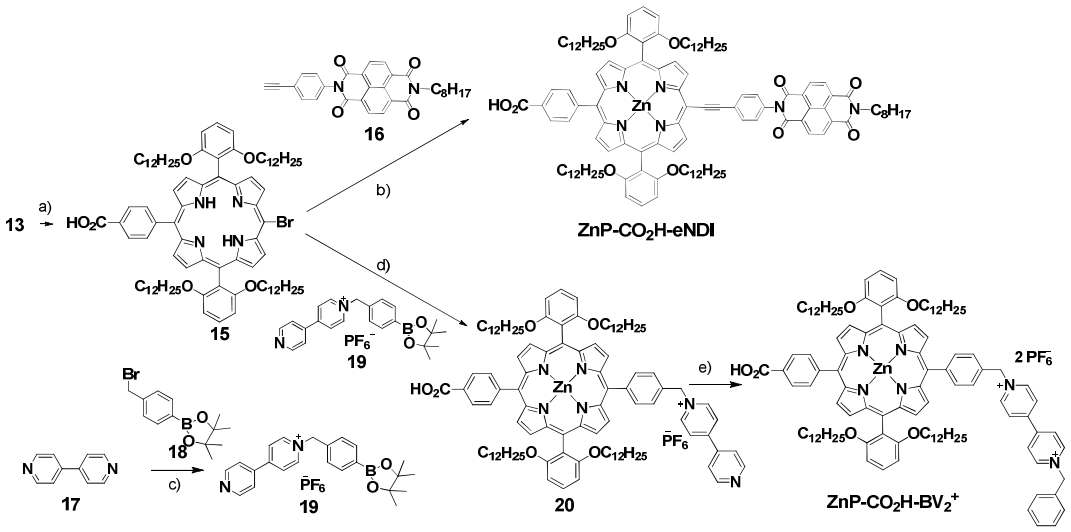

Scheme 3. Synthesis of the porphyrin ZnP-CO_2H-eNDI and ZnP-CO_2H-BV^{2+}. Reagents and conditions: a) NaOH (1M), THF/MeOH (v/v: 8/1), reflux; yield: 99%, b) $Zn(OAc)_2$.4 H_2O, CH_2Cl_2/MeOH (v/v: 1/1), reflux followed by $Pd(PPh_3)_4$, CuI, Et_3N, THF, reflux; yield: 68%, c) Tol, reflux; yield: 77%, d) $Zn(OAc)_2$.4 H_2O, CH_2Cl_2/MeOH (v/v: 1/1), reflux followed by $Pd(PPh_3)_4$, $Ba(OH)_2$.H_2O, THF/H_2O (v/v: 3/1), reflux; yield: 75%, e) BrBn, ACN/$CHCl_3$/MeOH, reflux; yield: 83%.

Electronic absorption and emission spectra

The electronic absorption spectra of the porphyrins, recorded in dichloromethane solution, are illustrated in Figure 1 and the spectroscopic data are gathered in Table 1.

View Article Online
DOI: 10.1039/C4TA05974C

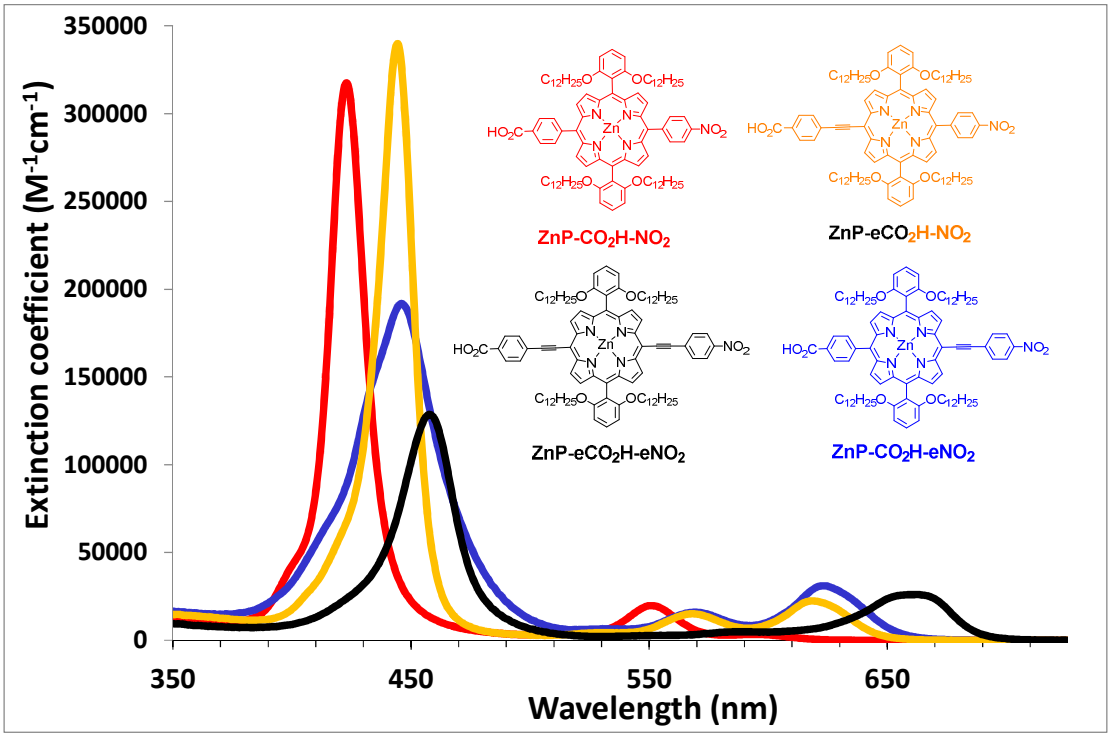

Figure 1. Overlay of the absorption spectra of the porphyrins **ZnP-CO_2H-NO_2**, **ZnP-eCO_2H-NO_2**, **ZnP-CO_2H-eNO_2** and **ZnP-eCO_2H-eNO_2** recorded in dichloromethane.

The spectrum of **ZnP-CO_2H-NO_2** features the classical π-π* transitions of regular tetraphenyl zinc porphyrin (ZnTPP). Indeed, we can easily distinguish an intense Soret band around 420 nm corresponding to a transition from the ground-state to higher excited-states and the two vibronic overtones of the Q-band between 500 and 600 nm attributed to the population of the lowest-lying excited states. The introduction of ethynyl moieties between the *meso* position of the porphyrin and the appended aryl substituents enhances the electronic communication, and this has two effects. First, it redshifts both the Soret and the Q-bands and second it inverses the relative intensities of the vibronic bands of the lowest-lying singlet excited state. These effects were previously rationalized in the studies of push-pull porphyrins designed for non-linear optical properties.[36, 37] Logically, these two effects are more pronounced on **ZnP-eCO_2H-eNO_2**, which carries two ethynyl moieties than in **ZnP-eCO_2H-NO_2** and **ZnP-CO_2H-eNO_2** which contain a single ethynyl substituent. Interestingly, for

View Article Online
DOI: 10.1039/C4TA05974C

ZnP-CO_2H-eNO_2 and **ZnP-eCO_2H-eNO_2** the Soret transition contains a significant charge transfer (CT) character corresponding to an electron shift from the ZnP core to the phenyl nitro group (see TD-DFT calculations below).

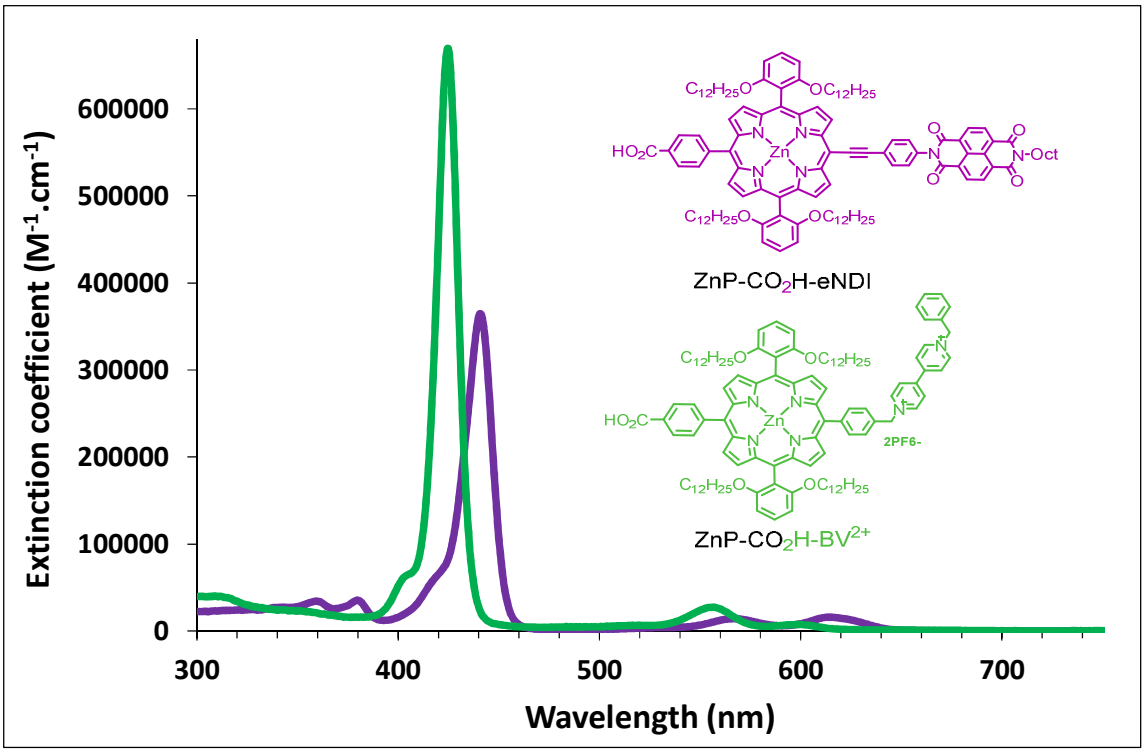

Figure 2. Overlay of the absorption spectra of the dyads **ZnP-CO_2H-BV^{2+}** and **ZnP-CO_2H-eNDI** recorded respectively in acetonitrile and dichloromethane solution.

The spectrum of **ZnP-CO_2H-BV^{2+}** is very similar to that of **ZnP-CO_2H-NO_2** in agreement with weak π electronic coupling of aryl groups with porphyrin macrocycle due to the phenyl-methylene linker between the porphyrin core and the viologen moiety. Concerning **ZnP-CO_2H-eNDI** dyad, the presence of the ethynyl group has the same effects as in the the monoethynyl porphyrin **ZnP-eCO_2H-NO_2** and **ZnP-CO_2H-eNO_2**: the peaks of the Soret and the Q-bands are shifted bathochromically by ~15 nm compared to the **ZnP-CO_2H-BV^{2+}** and their relative intensity are modified as described above. Additionally, the linked **NDI** unit presents its classical vibronic signature with two bands at 360 and

View Article Online
DOI: 10.1039/C4TA05974C

380 nm that indicate a weak electronic communication with the porphyrin core owing to the presence of nodes of the frontier molecular orbitals on the nitrogen of the imide groups.[38]

Table 1. Absorption and emission data of the porphyrins recorded in CH_2Cl_2 at room temperature.

Dyes	λ_{abs}/nm (ε/$M^{-1}cm^{-1}$)	λ_{em}/nm	E_{00} (eV)[a]
ZnP-CO_2H-NO_2	423 (317500); 551 (19700); 594 (3300)	601; 643	2.07
ZnP-eCO_2H-NO_2	444 (339800); 568 (15000); 619 (22400)	629; 680	1.99
ZnP-CO_2H-eNO_2	446 (191800); 570 (15900); 623 (31000)	630; 682	1.98
ZnP-eCO_2H-eNO_2	459 (127700); 558 (4800); 660 (26000)	664; 730	1.87
ZnP-CO_2H-eNDI	342.5 (28000);359.5 (35000); 379.5 (35000); 441 (364000); 567 (14000); 614 (16000)	625.5; 670	2.00
ZnP-CO_2H-BV^{2+}	425 (670000); 557 (28000); 600 (7000)	610; 662	2.09

[a]calculated with the wavelength at the intersection of the absorption and emission spectra (λ_{inter}) according to the equation: $E_{00} = 1240/\lambda_{inter}$

All porphyrins are fluorescent dyes and this feature enables to determine the zero-zero transition energy (E_{00}) between the ground state and the first singlet excited state from the wavelength at the intersection of the absorption and emission spectra (Table 1). Expectedly, the fluorescence of **ZnP-CO_2H-BV^{2+}** and **ZnP-CO_2H-aNDI** is significantly quenched, most probably by photoinduced electron transfer from ZnP to the adjacent electron acceptor (BV^{2+} or NDI), as previously observed in similar systems.[39-42]

TD-DFT calculations

To shed some light on the electronic properties of these sensitizers, TD-DFT quantum chemical calculations were undertaken. First the theoretical calculations confirm the large twisting angles

View Article Online
DOI: 10.1039/C4TA05974C

between the ZnP core and the side phenyl ring when no ethynyl segment is added. Indeed, the DFT optimizations return a nearly perfectly planar conjugated path in **ZnP-eCO$_2$H-eNO$_2$** whereas, the dihedral angles between the ZnP and the phenyl ring attain 64° (carboxylic side) and 62° (nitro side) in **ZnP-CO$_2$H-NO$_2$**. Table 2 lists the main computed data, whereas Figure 3 provides a graphical representation of the frontier orbitals. For the electronic absorption, TD-DFT predicts that the Q-band is shifted by +32 nm (+34 nm) and becomes 6.4 (7.9) times more intense when going from **ZnP-CO$_2$H-NO$_2$** to **ZnP-eCO$_2$H-NO$_2$** (**ZnP-CO$_2$H-eNO$_2$**) and this fits the experimental data of Table 1, where the corresponding wavelength and intensity effects are +25 nm (+29 nm) and x6.7 (x9.4), respectively. Likewise compound with the two ethynyl segments, **ZnP-eCO$_2$H-eNO$_2$**, yields the most red-shifted Q-band in both theory and experiment with a bathochromic shift of +66 nm (measurements) and +78 nm (theory) compared to **ZnP-CO$_2$H-NO$_2$**. The positions of the Soret band are also reasonably reproduced by the calculations, hinting that the selected theoretical model is suited for our purposes. As can be seen in Figure 3, the HOMO is systematically mainly localized on the central ZnP core though it is slightly delocalized on the adjacent ethynyl segments when they are present. Consistently with the electrochemical measurements the energies of these HOMO orbitals are quite constant but for **ZnP-CO$_2$H-BV^{2+}** where a significant stabilization is projected, probably due to the presence of the dicationic moiety close to the ZnP. The LUMO of the four monomeric species are localized on the porphyrin core as well as on the side *p*-nitro-phenyl group, irrespective of the presence of an ethynyl linker separating them. In the dyads, the LUMO are, as expected, fully located on the secondary acceptors. As can be seen from Table 2, the energy of the LUMO decreases when one adds ethynyl segments. While it is logically lower with the **NDI** fragment, it is strongly stabilized for the **BV^{2+}** which could be problematic for the regeneration process.

View Article Online
DOI: 10.1039/C4TA05974C

Table 2. Computed data for the lowest-lying excited-states corresponding to Q and Soret bands for all dyes. The computed wavelengths reported are for the first four excited-states (λ_{abs} in nm) and their oscillator strengths (f in a.u.) as well as the energies of the HOMO and LUMO (in eV), as well as the ground-state dipole moments (μ in D).

Dyes	λ_{abs} (f)	HOMO	LUMO	μ
ZnP-CO_2H-NO_2	390 (1.563); 402 (1.698); 556 (0.002); 564 (0.057)	-6.29	-1.93	5.14
ZnP-eCO_2H-NO_2	402 (1.478); 413 (2.373); 571 (0.003); 596 (0.364)	-6.24	-2.15	3.35
ZnP-CO_2H-eNO_2	403 (1.409); 428 (2.099); 571 (0.005); 598 (0;452)	-6.25	-2.24	7.74
ZnP-eCO_2H-eNO_2	411 (1.361); 426 (2.296); 588 (0.024); 642 (0.857)	-6.21	-2.43	5.82
ZnP-CO_2H-eNDI	400 (1.550); 407 (2.579); 569 (0.000); 590 (0.306)	-6.15	-2.61	2.06
ZnP-CO_2H-BV^{2+}	387 (1.708); 391 (2.113); 557 (0.004); 564 (0.048)	-6.48	-3.18	[a]

[a]not significant (charged compound due to the neglect of the counterions in the calculations)

View Article Online
DOI: 10.1039/C4TA05974C

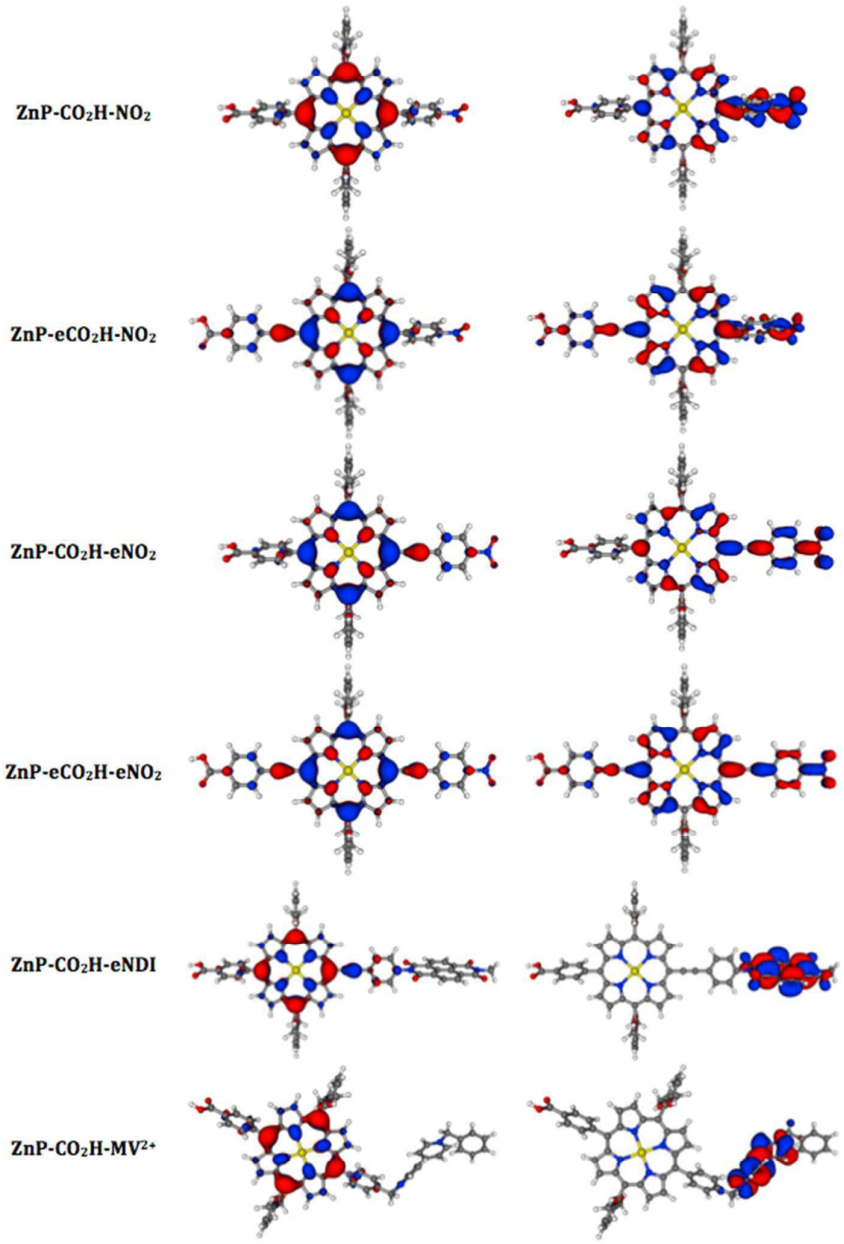

Figure 3. Representation of the frontier orbitals (Left: HOMO, right: LUMO) for the six investigated systems.

To check if the extension of the LUMO to the nitro group has also a strong influence on the properties of the excited-states, the density difference plots for two representative dyes were computed with and without ethynyl linker between the ZnP and the *p*-nitro-phenyl group. The results are given in Figure 4 for the first Soret band. As can be seen, in both cases, there is a strong charge

View Article Online
DOI: 10.1039/C4TA05974C

transfer (CT) from the porphyrin to the electron-acceptor. The computed charge-transfer distances are 4.92 Å and 5.05 Å for the two cases, respectively. This clearly hints that the CT does not disappear when the ethynyl segment is removed.

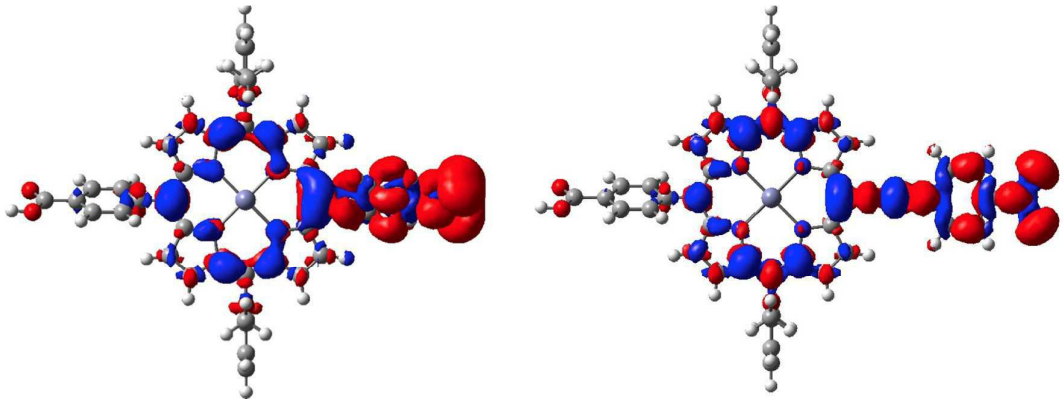

Figure 4. Representation density difference plots (red: increase of density, blue: decrease of density) between the first Soret excited-state and the ground-state for **ZnP-CO_2H-NO_2** (left) and **ZnP-CO_2H-eNO_2** (right).

Electrochemical characterization

To estimate the driving force of the photoinduced hole transfer into NiO valence band (ΔG_{inj}) and that of the dye regeneration reaction (ΔG_{reg}), the redox potentials of the porphyrins were recorded by cyclic voltammetry and differential pulse voltammetry in dichloromethane. The values of the Gibbs free-energy change of these processes are listed in Table 2. The oxidation potential of the zinc porphyrin is not much affected by the substituents, while the reduction process becomes easier as the nitro-phenyl substituent is appended through an ethynyl moiety (**ZnP-CO_2H-eNO_2** and **ZnP-eCO_2H-eNO_2**). In the dyads, the oxidation process lies on the zinc porphyrin macrocycle, while the first reduction process occurs at a more positive potential than that of ZnP localized on the adjacent secondary electron acceptor (NDI or BV^{2+}) due to its better electron acceptor capability (between 250 and 400 mV). Accordingly, there is a significant driving force to shift the electron from the reduced

View Article Online
DOI: 10.1039/C4TA05974C

zinc porphyrin to the secondary electron acceptor. The reduction process localized on the porphyrin moiety in the dyads occurs at more cathodic potentials than push-pull ones because of the presence of the already reduced secondary electron acceptor.

Table 3. Redox potentials of the porphyrins recorded in CH_2Cl_2 and referenced versus saturated calomel electrode (SCE).

Dyes	$E_{Ox}(P^+/P)$	$E_{Red}(P/P^-)$	$E_{Red}(NDI/NDI^-)$ or $E_{Red}(BV^{2+}/BV^+)$	$E_{Red}(P^*/P^-)$[a]	ΔG_{inj} (eV)[b]	ΔG_{reg} (eV)[c]
ZnP-CO_2H-NO_2	+ 0.72	- 1.14	/	+ 0.93	- 0.63	- 0.82
ZnP-eCO_2H-NO_2	+ 0.77	- 1.12	/	+ 0.87	- 0.57	- 0.82
ZnP-CO_2H-eNO_2	+ 0.74	- 1.07	/	+ 0.91	- 0.61	- 0.75
ZnP-eCO_2H-eNO_2	+ 0.75	- 1.05	/	+ 0.82	- 0.52	- 0.73
ZnP-CO_2H-eNDI	+ 0.75	-1.46	-0.59	+ 0.54	- 0.24	- 0.27
ZnP-CO_2H-BV^{2+}	+ 0.73	-1.52	-0.21	+ 0.57	- 0.27	+ 0.11

[a]calculated according to the equation: $E_{Red}(P^*/P^-) = E_{Red}(P/P^-) + E_{00}$. [b]calculated according to the equation: $\Delta G_{inj} = E_{VB}(NiO) - E_{Red}(P^*/P^-)$ with $E_{VB}(NiO)$ standing for the potential of the valence band of NiO and taken as 0.3 V vs SCE. [c]calculated according to the equation: $\Delta G_{reg} = E_{Red}(A/A^-) - E(I_3^-/I_2^{-\bullet})$, with $E(I_3^-/I_2^{-\bullet})$ taken as - 0.32 V vs SCE and A = porphyrin for ZnP-CO_2H-NO_2 derivatives and NDI or BV^{2+} for ZnP-CO_2H-eNDI or ZnP-CO_2H-MV^2 respectively.

An energy diagram of the dyes energy levels along with that of the VB of NiO and redox mediators is drawn in Figure 5. It enables to visually observe that, for all presented dyes, there is significant exergonicity to inject a hole in NiO (~400 mV). Concerning the regeneration process, all push-pull dyes and dyad **ZnP-CO_2H-eNDI** exhibit a large driving force to oxidize the reduced sensitizer by the redox mediator for all the porphyrin sensitizers. However, the regeneration driving force for dyad **ZnP-CO_2H-BV^{2+}** is slightly endergonic rending this process certainly sluggish. In summary, aside from the latter dyad **ZnP-CO_2H-BV^{2+}**, all the others dyes satisfy the thermodynamic criteria to act as

View Article Online
DOI: 10.1039/C4TA05974C

efficient sensitizer of NiO in p-DSCs because both injection and regeneration reactions are exergonic processes.

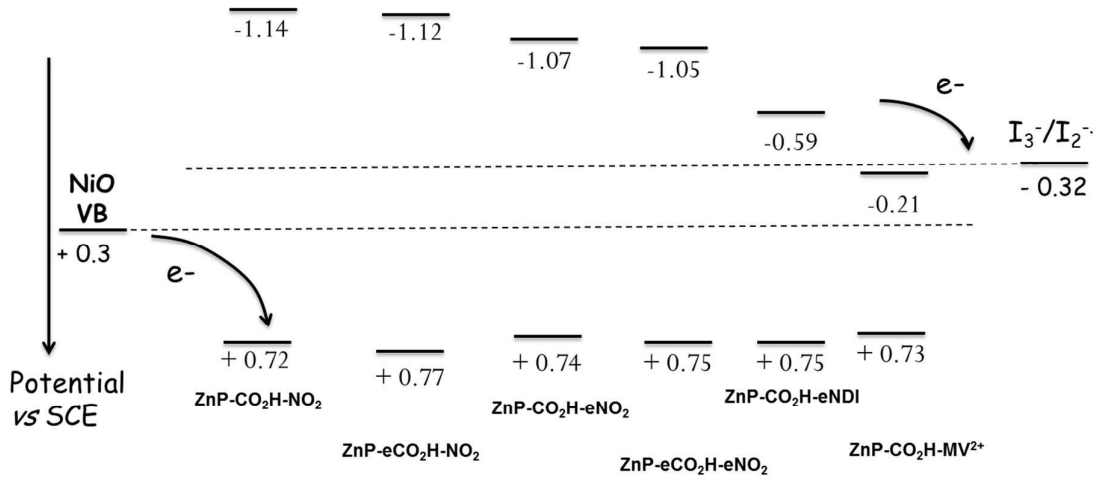

Figure 5. Energy diagram of the relevant levels for the hole photoinjection and dye regeneration reactions in NiO based DSC.

Photovoltaic performances on NiO

These porphyrin systems were used as sensitizers in nanocrystalline NiO-based photocathodes using the iodide/triiodide couple as redox shuttle (see experimental part for details). The short current photocurrent density (J_{SC}), open circuit voltage (V_{OC}), fill factor (ff) and photoconversion efficiency (η) recorded under stimulated AM1.5G solar light (100 mW/cm^2) are listed in Table 4. The action spectra of the incident photo-to-current conversion efficiency (IPCE) as a function of the incident wavelength of the p-DSCs sensitized with the porphyrin dyes are shown in Figures 5 and 6.

View Article Online
DOI: 10.1039/C4TA05974C

Table 4. Photovoltaic characteristics of the solar cells made with mesoporous NiO electrodes sensitized with the porphyrin dyes using I^-/I_3^- electrolyte and recorded under stimulated AM1.5G solar light (100 mW/cm^2).

Dyes	J_{SC} (mA/cm^2)	V_{OC} (mV)	ff (%)	η (%)
ZnP-CO_2H-NO_2	0.49	113	36	0.020
ZnP-eCO_2H-NO_2	0.48	114	35	0.019
ZnP-CO_2H-eNO_2	0.43	98	32	0.013
ZnP-eCO_2H-eNO_2	0.55	115	34	0.022
ZnP-CO_2H-eNDI	1.38	127	32	0.056
ZnP-CO_2H-BV^{2+}	0.44	125	33	0.018

Unexpectedly, the four monomeric porphyrins give modest and relatively similar photovoltaic performances, with Jsc around 0.5 mA/cm^2 and Voc around 110 mV. Consistent with the J/V curves, the photoaction spectra of the monomeric dyes indicate very low values of IPCE on the absorption bands of the porphyrins with almost no photoactivity on the Q-bands (Figure 5). These results indicate that the presence of ethynyl moieties between the aryl substituents and the porphyrin core has a little impact of the photovoltaic performances and, obviously, does not control them in a first extent. However, **ZnP-eCO_2H-eNO_2** exhibits the higher IPCE value on the Q band compare to the other monomeric ZnPs. This is certainly the consequence of the higher extinction coefficient of **ZnP-eCO_2H-eNO_2** on this band. The calculated hole injection and regeneration driving forces are particularly large for these series of dyes (Table 2) suggesting that kinetic is rather the limiting factor than thermodynamic. Indeed, it was demonstrated with different classes of dyes that hole injection from the dye excited-state is rather a fast process (with tens of ps and even faster), while charge recombination between the injected hole in NiO and the reduced sensitizer is also an unusually very

View Article Online
DOI: 10.1039/C4TA05974C

fast process (ns time-scale and sometimes faster).[18, 42-46] This fast charge recombination strongly limits the photocurrent density as it outcompetes with the reduction of the electrolyte by the reduced sensitizer and is a general bottleneck in p-DSCs.[8] The fast charge recombination in these series of monomeric ZnP is well supported with the extended delocalization of the LUMO on the porphyrin macrocycle, whatever the structure of the porphyrin (Figure 3). In these systems, upon reduction the electron on the porphyrin certainly significantly interacts with the NiO VB, because there is a significant spin density of the LUMO at proximity and quite the same distance to the NiO surface for all the monomeric porphyrins. Accordingly, the charge recombination with NiO is certainly very fast and quite similar for all ZnP of the first series. This hypothesis is also consistent with the higher J_{SC} recorded with the dyad **ZnP-CO$_2$H-eNDI** sensitizer (Table 3) and the recent result reported by Sun and co-workers using a ZnP linked to a fullerene derivative acting as secondary electron acceptor.[20] In addition, it was previously demonstrated that dyad systems in the form of "S-A" with S=sensitizer and A=secondary acceptor exhibit much longer lived charge separated states and gave higher photovoltaic performances, owing to the electronic decoupling and the increased distance between the hole (in NiO) and the electron (on the secondary acceptor).[10, 11, 26, 45] Consistent with these previous studies, the dyad **ZnP-CO$_2$H-eNDI** effectively gave higher J_{SC} than monomeric porphyrins (Table 3).[25, 26] On the contrary and as expected by the electrochemical characterization, the presence of the viologen as a secondary electron acceptor in the dyad **ZnP-CO$_2$H-BV^{2+}** exhibits poor photovoltaic performances. This is certainly due to the endergonic regeneration process related to the very low reduction potential of the benzyl viologen unit (E_{Red} = -0.21 vs. SCE, Table 2) which impedes the performances of the **BV^{2+}**-based dyad. Interestingly, the Q-bands of the porphyrin in **ZnP-CO$_2$H-eNDI** are effectively active to produce electricity as IPCE value as much as 16% can be measured at 630 nm (Figure 4), showing the potential of ZnP-acceptor dyads for p-DSCs. Finally, the best performing system **ZnP-CO$_2$H-eNDI** was tested with the cobalt electrolyte, which is only compatible with long-lived charge separated state.[11, 26, 47] Interestingly, this compound is suited with this electrolyte as the solar cell using the dyad **ZnP-CO$_2$H-eNDI** gave the following characteristics: J_{SC}=

View Article Online
DOI: 10.1039/C4TA05974C

0,5 mA/cm^2, V_{OC} = 195 mV, ff= 31 % , η= 0.03 %. These results attest of the significantly long-lived charge separated state formed within **ZnP-CO$_2$H-eNDI**, though the performances are not as high as in other dyads.[11, 48] Particularly, the V_{OC} is lower than the usually measured value with this electrolyte (around 300 mV). This can be ascribed to the shorter lived charge separated state than previously reported dyads.

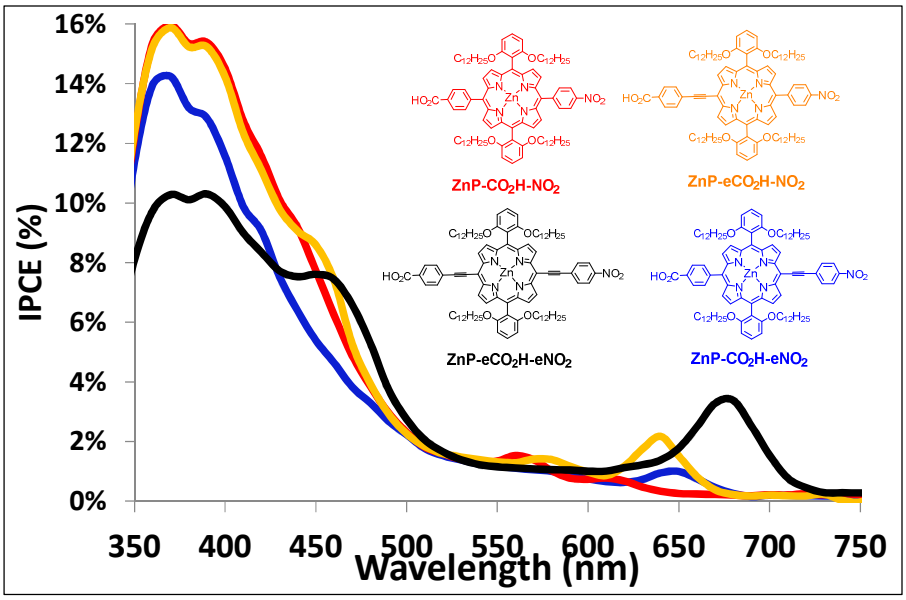

Figure 6. IPCE spectra of the p-DSCs devices sensitized with the four monomeric porphyrin dyes using the I^-/I_3^- electrolyte.

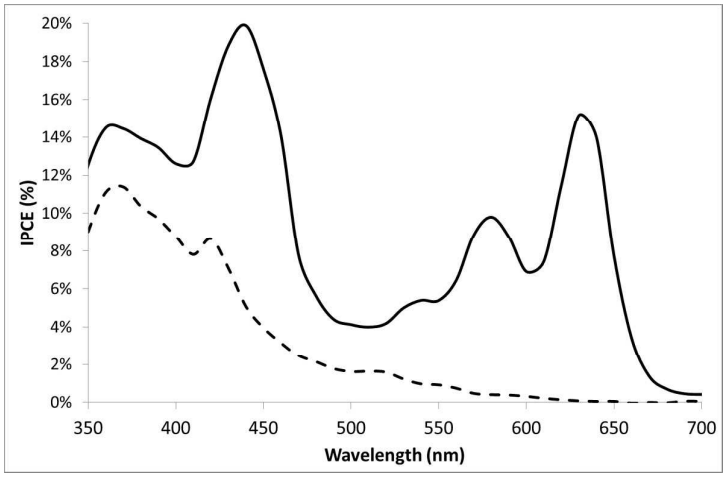

View Article Online
DOI: 10.1039/C4TA05974C

Figure 7. IPCE spectra of the p-DSCs devices sensitized with the dyads **ZnP-CO_2H-eNDI** (solid line) and **ZnP-CO_2H-BV^{2+}** (dashed line) using the I^-/I_3^- electrolyte.

Conclusions

In summary, we have synthesized and investigated the properties in NiO based p-DSC of two new series of porphyrin sensitizers. The first series consists in push-pull zinc porphyrins incorporating or not an ethynyl spacer between the *trans meso* aryl groups and the porphyrin core. In the second series of systems, a benzyl viologen or a NDI have been appended to the ZnP as secondary electron acceptor. The optical and electrochemical properties of these sensitizers were experimentally elucidated and quantum chemical calculations were performed to rationalize their electronic properties. We showed that in spite of the favorable charge transfer characteristics along with the large energy changes of the injection and regeneration reactions, the first series of push-pull monomeric zinc porphyrins yield relatively low photocurrent density in p-DSC. This is in sharp contrast to parent push-pull zinc porphyrins, which give outstanding photovoltaic performances in conventional TiO_2 based DSCs.[3, 4, 14, 49] The modest J_{SC} measured with these monomeric ZnP was ascribed to the fast charge recombination owing to the partial delocalization of the electron density close to the surface. By the introduction of a secondary electron acceptor next to the porphyrin (second series of sensitizers) the performances were significantly improved, most probably because the electron is shifted from the ZnP to the secondary acceptor, and this slows down the charge recombination. As a consequence, one dyad (**ZnP-CO_2H-eNDI**) was shown to be compatible with the cobalt electrolyte. This study demonstrates that simple push-pull porphyrins need further molecular optimizations in order to reach higher efficiencies in p-DSCs. More precisely, the charge recombination must be slowed down by either changing the nature of the anchoring group and/or of the spacer linking the porphyrin to the NiO surface. Another possibility is to introduce new electron acceptor in the vicinity of the porphyrin. These information are certainly crucial to pave the way to

View Article Online
DOI: 10.1039/C4TA05974C

the development of better performing porphyrin based sensitizers for NiO DSCs, which, in our views, remains a very promising class of dye for such applications.

Acknowledgments

ANR is gratefully acknowledged for the financial support of these researches through the program POSITIF (ANR-12-PRGE-0016-01), CNRS, Région des Pays de la Loire for the projects NiOPhotoCat and LUMOMAT, and COST CM1202 program (PERSPECT H2O). F. B. A. is indebted to the Région des Pays de la Loire for his PhD grant. D. J. acknowledges both the European Research Council (ERC) and the Région des Pays de la Loire for financial support in the framework of a Starting Grant (Marches – 278845) and a recrutement sur poste stratégique, respectively. This research used resources of (1) the GENCI-CINES/IDRIS (Grant c2014085117) and (2) CCIPL (Centre de Calcul Intensif des Pays de Loire).

Electronic supplementary information (ESI) available:

Experimental procedures for the synthesis of the new compounds. See DOI: xxxxx.

References:

1. A. Hagfeldt, G. Boschloo, L. Sun, L. Kloo and H. Pettersson, *Chem. Rev.*, 2010, **110**, 6595.
2. F. Odobel, L. Le Pleux, Y. Pellegrin and E. Blart, *Acc. Chem. Res.*, 2010, **43**, 1063.
3. S. Mathew, A. Yella, P. Gao, R. Humphry-Baker, F. E. CurchodBasile, N. Ashari-Astani, I. Tavernelli, U. Rothlisberger, K. NazeeruddinMd and M. Grätzel, *Nat. Chem.*, 2014, **6**, 242.
4. A. Yella, H.-W. Lee, H. N. Tsao, C. Yi, A. K. Chandiran, M. K. Nazeeruddin, E. W.-G. Diau, C.-Y. Yeh, S. M. Zakeeruddin and M. Grätzel, *Science*, 2011, **334**, 629.
5. H. J. Snaith, *Journal of Physical Chemistry Letters*, 2013, **4**, 3623.
6. G. Li, R. Zhu and Y. Yang, *Nat. Photon.*, 2012, **6**, 153.
7. Y.-J. Cheng, S.-H. Yang and C.-S. Hsu, *Chem. Rev.*, 2009, **109**, 5868.
8. F. Odobel, Y. Pellegrin, E. A. Gibson, A. Hagfeldt, A. L. Smeigh and L. Hammarström, *Coord. Chem. Rev.*, 2012, **256**, 2414.

View Article Online
DOI: 10.1039/C4TA05974C

9. F. Odobel and Y. Pellegrin, *J. Phys. Chem. Lett.*, 2013, **4**, 2551.

10. A. Nattestad, A. J. Mozer, M. K. R. Fischer, Y. B. Cheng, A. Mishra, P. Baeuerle and U. Bach, *Nat. Mater.*, 2010, **9**, 31.

11. E. A. Gibson, A. L. Smeigh, L. L. Pleux, J. Fortage, G. Boschloo, E. Blart, Y. Pellegrin, F. Odobel, A. Hagfeldt and L. Hammarström, *Angew. Chem. Int. Ed.*, 2009, **48**, 4402.

12. J. He, H. Lindström, A. Hagfeldt and S. E. Lindquist, *Sol. Energy Mater. Sol. Cells* 2000, **62**, 265.

13. A. Nakasa, H. Usami, S. Sumikura, S. Hasegawa, T. Koyama and E. Suzuki, *Chem. Lett.*, 2005, **34**, 500.

14. L.-L. Li and E. W.-G. Diau, *Chem. Soc. Rev.*, 2013, **42**, 291.

15. H. Imahori, T. Umeyama and S. Ito, *Acc. Chem. Res.*, 2009, **42**, 1809.

16. H. Qin, L. Li, F. Guo, S. Su, J. Peng, Y. Cao and X. Peng, *Energy Environ. Sci.*, 2014, **7**, 1397.

17. Y. I. H. Chao, J.-F. Jheng, J.-S. Wu, K.-Y. Wu, H.-H. Peng, M.-C. Tsai, C.-L. Wang, Y.-N. Hsiao, C.-L. Wang, C.-Y. Lin and C.-S. Hsu, *Adv. Mater.*, 2014, **26**, 5205.

18. M. Borgström, E. Blart, G. Boschloo, E. Mukhtar, A. Hagfeldt, L. Hammarström and F. Odobel, *J. Phys. Chem. B*, 2005, **109**, 22928.

19. J. He, H. Lindström, A. Hagfeldt and S.-E. Lindquist, *J. Phys. Chem. B*, 1999, **103**, 8940.

20. H. Tian, J. Oscarsson, E. Gabrielsson, S. K. Eriksson, R. Lindblad, B. Xu, Y. Hao, G. Boschloo, E. M. J. Johansson, J. M. Gardner, A. Hagfeldt, H. Rensmo and L. Sun, *Sci. Rep.*, 2014, **4**.

21. M. Amaresh, K. R. F. Markus and B. Peter, *Angew. Chem. Int. Ed.*, 2009, **48**, 2474.

22. P. Qin, H. Zhu, T. Edvinsson, G. Boschloo, A. Hagfeldt and L. Sun, *J. Am. Chem. Soc.*, 2008, **130**, 8570.

23. F. Odobel, Y. Pellegrin, F. B. Anne and D. Jacquemin, in *High-Efficiency Solar Cells - Physics, Materials and Devices*, ed. Z. M. W. a. X. Wang, Springer, 2013.

24. Y.-C. Chang, C.-L. Wang, T.-Y. Pan, S.-H. Hong, C.-M. Lan, H.-H. Kuo, C.-F. Lo, H.-Y. Hsu, C.-Y. Lin and E. W.-G. Diau, *Chem. Commun.*, 2011, **47**, 8910.

25. L. Favereau, J. Warnan, Y. Pellegrin, E. Blart, M. Boujtita, D. Jacquemin and F. Odobel, *Chem. Commun.*, 2013, **49**, 8018.

26. L. Le Pleux, A. L. Smeigh, E. Gibson, Y. Pellegrin, E. Blart, G. Boschloo, A. Hagfeldt, L. Hammarström and F. Odobel, *Energy Environ. Sci.*, 2011, **4**, 2075.

27. M. J. Frisch, G. W. Trucks, H. B. Schlegel, G. E. Scuseria, M. A. Robb, J. R. Cheeseman, G. Scalmani, V. Barone, B. Mennucci, G. A. Petersson, H. Nakatsuji, M. Caricato, X. Li, H. P. Hratchian, A. F. Izmaylov, J. Bloino, G. Zheng, J. L. Sonnenberg, M. Hada, M. Ehara, K. Toyota, R. Fukuda, J. Hasegawa, M. Ishida, T. Nakajima, Y. Honda, O. Kitao, H. Nakai, T. Vreven, Jr, J.

View Article Online
DOI: 10.1039/C4TA05974C

E. Peralta, F. Ogliaro, M. Bearpark, J. J. Heyd, E. Brothers, K. N. Kudin, V. N. Staroverov, R. Kobayashi, J. Normand, K. Raghavachari, A. Rendell, J. C. Burant, S. S. Iyengar, J. Tomasi, M. Cossi, N. Rega, J. M. Millam, M. Klene, J. E. Knox, J. B. Cross, V. Bakken, C. Adamo, J. Jaramillo, R. Gomperts, R. E. Stratmann, O. Yazyev, A. J. Austin, R. Cammi, C. Pomelli, J. W. Ochterski, R. L. Martin, K. Morokuma, V. G. Zakrzewski, G. A. Voth, P. Salvador, J. J. Dannenberg, S. Dapprich, A. D. Daniels, Farkas, J. B. Foresman, J. V. Ortiz, J. Cioslowski and D. J. Fox, *Gaussian 09 Revision A.02*, Gaussian Inc. Wallingford CT 2009, 2009.

28. C. Adamo and V. Barone, *J. Chem. Phys.*, 1999, **110**, 6158.

29. T. Yanai, D. P. Tew and N. C. Handy, *Chem. Phys. Lett.*, 2004, **393**, 51.

30. T. Le Bahers, C. Adamo and I. Ciofini, *J. Chem. Theory Comput.*, 2011, **7**, 2498.

31. J. Tomasi, B. Mennucci and R. Cammi, *Chem. Rev.*, 2005, **105**, 2999.

32. C. Yi, F. Giordano, N.-L. Cevey-Ha, H. N. Tsao, S. M. Zakeeruddin and M. Graetzel, *Chem. Sus. Chem.*, 2014, **7**, 1107.

33. R. W. Wagner, T. E. Johnson, F. Li and J. S. Lindsey, *J. Org. Chem.*, 1995, **60**, 5266.

34. L. Favereau, J. Warnan, F. B. Anne, Y. Pellegrin, E. Blart, D. Jacquemin and F. Odobel, *J. Mater. Chem. A*, 2013, **1**, 7572.

35. F. Chaignon, M. Falkenstrom, S. Karlsson, E. Blart, F. Odobel and L. Hammarstrom, *Chem. Commun.*, 2007, **0**, 64.

36. T.-G. Zhang, Y. Zhao, I. Asselberghs, A. Persoons, K. Clays and M. J. Therien, *J. Am. Chem. Soc.*, 2005, **127**, 9710.

37. S. Priyadarshy, M. J. Therien and D. N. Beratan, *J. Am. Chem. Soc.*, 1996, **118**, 1497.

38. F. Chaignon, M. Falkenstroem, S. Karlsson, E. Blart, F. Odobel and L. Hammarström, *Chem. Commun.*, 2007, 64.

39. S. Wallin, C. Monnereau, E. Blart, J.-R. Gankou, F. Odobel and L. Hammarstrom, *J. Phys. Chem. A*, 2010, **114**, 1709.

40. S. Noda, H. Hosono, I. Okura, Y. Yamamoto and Y. Inoue, *Faraday Trans.*, 1990, **86**, 811.

41. I. Okura and H. Hosono, *J. Phys. Chem.*, 1992, **96**, 4466.

42. A. Morandeira, J. Fortage, T. Edvinsson, L. Le Pleux, E. Blart, G. Boschloo, A. Hagfeldt, L. Hammarström and F. Odobel, *J. Phys. Chem. C*, 2008, **112**, 1721.

43. A. Morandeira, G. Boschloo, A. Hagfeldt and L. Hammarström, *J. Phys. Chem. B*, 2005, **109**, 19403.

44. A. L. Smeigh, L. L. Pleux, J. Fortage, Y. Pellegrin, E. Blart, F. Odobel and L. Hammarström, *Chem. Commun.*, 2012, **48,** , 678.

View Article Online
DOI: 10.1039/C4TA05974C

45. J. Warnan, J. Gardner, L. Le Pleux, J. Petersson, Y. Pellegrin, E. Blart, L. Hammarström and F. Odobel, *J. Phys. Chem. C*, 2013, **118**, 103.

46. P. Qin, J. Wiberg, E. A. Gibson, M. Linder, L. Li, T. Brinck, A. Hagfeldt, B. Albinsson and L. Sun, *J. Phys. Chem. C* 2010, **114**, 4738.

47. E. A. Gibson, A. L. Smeigh, L. Le Pleux, L. Hammarström, F. Odobel, G. Boschloo and A. Hagfeldt, *J. Phys. Chem. C* 2011, **115**, 9772.

48. L. Favereau, J. Warnan, Y. Pellegrin, E. Blart, M. Boujtita, D. Jacquemin and F. Odobel, *Chem. Commun.*, 2013, **49**, 8018.

49. Y.-C. Chang, C.-L. Wang, T.-Y. Pan, S.-H. Hong, C.-M. Lan, H.-H. Kuo, C.-F. Lo, H.-Y. Hsu, C.-Y. Lin and E. W.-G. Diau, *Chem. Commun.*, 2011, **47**, 8910.

View Article Online
DOI: 10.1039/C4TA05974C

Graphical abstract for entry

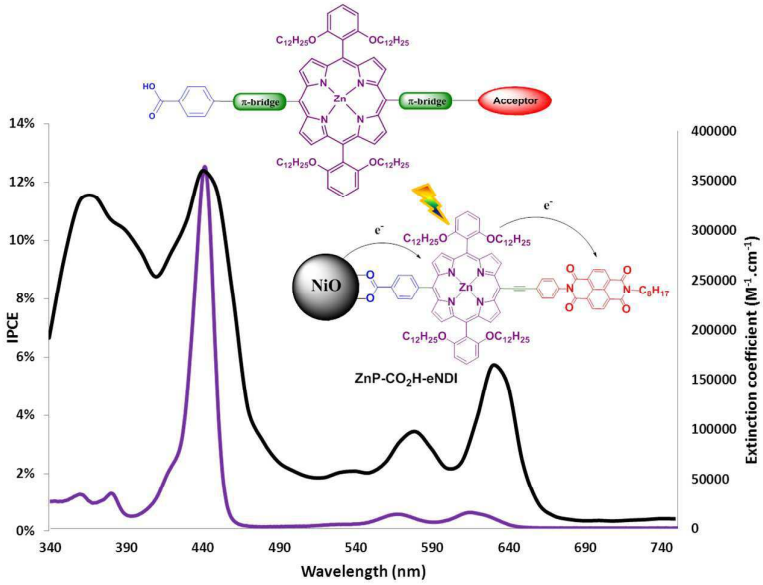

Push-pull zinc porphyrins can be suitable sensitizers for NiO-based p-DSSCs provided that geminate charge recombination is minimized.